nature catalysis

Analysis

https://doi.org/10.1038/s41929-025-01339-0

Understanding two voltammetric features of water reduction and water oxidation in mild pH solutions

Received: 5 March 2024

Accepted: 8 April 2025

Published online: 14 May 2025

Check for updates

Xin Yuan[1,2], Michael T. Bender[1,2], Myohwa Ko[1] & Kyoung-Shin Choi[1]

Electrification of many processes requires the use of aqueous solutions under mild pH conditions where the hydrogen evolution reaction (HER) and the oxygen evolution reaction (OER) can become competing reactions. The HER and OER under mild pH conditions show peculiar voltammetric behaviours, specifically two reductive or oxidative features, that are not observed in strongly acidic and basic solutions. These behaviours cannot be fully explained by thermodynamic considerations only and are particularly complex owing to the involvement of multiple water species (H_3O^+, H_2O and OH^-) and the conversion between these species via water autodissociation and acid–base neutralization reactions. This Analysis provides a systematic and conceptual explanation of the effect of pH, potential, stirring and buffer on the thermodynamics and kinetics of the HER and OER, providing fundamental and yet essential insights into comprehending HER and OER behaviours under mild pH conditions, and their implications for other aqueous reactions more broadly.

The reduction of water to H_2 (hydrogen evolution reaction, HER) and the oxidation of water to O_2 (oxygen evolution reaction, OER) are among the most important and well-studied electrochemical reactions[1–3]. They are the reactions used for water splitting (or water electrolysis) through which H_2 is produced as a clean fuel. For water electrolysis to obtain H_2, strongly acidic and basic solutions have typically been used to maintain high concentrations of H^+ and OH^-, which offers a high solution conductivity without needing a buffer or supporting electrolyte and enhances the rate of the HER and OER.

Recently, electrification of various processes, that is, achieving these processes electrochemically using renewable electricity, is attracting considerable attention because it can offer greener and more sustainable approaches to chemical production while reducing CO_2 emissions[4–7]. Many of these processes need an electrolyte with a mild pH to increase the stability and solubility of reactants and products, to increase the product selectivity and/or to increase the Faradaic efficiency of the desired reaction[7–11]. For these processes, the HER and OER can become competing reactions or are used as the counter-electrode reaction. Thus, understanding the HER and OER under mild pH conditions is critical to optimizing these processes. Surprisingly, our understanding of the HER and OER under mild pH conditions has been very limited because it is often assumed that there is nothing unique about these reactions compared to how they behave in strongly acidic and basic media other than the shift of the onset potentials predicted by thermodynamics using the Nernst equation. Because the concentrations of H_3O^+ and OH^- are limited in mild pH solutions, this assumption means that reduction of H_3O^+ versus H_2O and oxidation of OH^- versus H_2O are indistinguishable. This in turn means that all these reactions are very fast and are under thermodynamic control, and there is no need to consider differences in the kinetics of H_3O^+ versus H_2O reduction or OH^- versus H_2O oxidation or effects caused by the ability to deplete H_3O^+ and OH^- but not H_2O. However, the HER and OER under mild pH conditions show puzzling voltammetric behaviours, specifically two reductive or oxidative features, not observed in strongly acidic and basic media, which are regularly misinterpreted by researchers. The complexities of the HER and OER in mild pH solutions cannot be fully

[1]Department of Chemistry, University of Wisconsin–Madison, Madison, WI, USA. [2]These authors contributed equally: Xin Yuan, Michael T. Bender.
e-mail: kschoi@chem.wisc.edu

understood by previous studies that compare these reactions only in strongly acidic and strongly basic solutions or that do not distinguish different cases created by kinetic variations between H_3O^+ reduction and H_2O reduction or between OH^- oxidation and H_2O oxidation.

The goal of this Analysis is to systematically demonstrate when and why the two HER and OER features appear at mild pH conditions and discuss the effect of pH, applied potential, stirring, buffer and the catalytic ability of the electrode on these behaviours. In doing so, this Analysis provides a unique opportunity to reflect on the meaning of the Nernst equation (that is, the thermodynamic relationship between the applied potential and the equilibrium pH at the electrode surface), potential-dependent rate constants for the HER and OER, and the complexity of the HER and OER associated with water dissociation and acid–base neutralization reactions at the electrode surface. We will first provide an in-depth discussion of the HER and show how the OER mirrors it. Then we will present a case study showing how understanding the two OER features in a mildly basic solution is important to accurately interpret results obtained from other aqueous reactions.

Results

HER in acidic, basic and neutral conditions

The HER in acidic and basic solutions and the corresponding Nernst equations, assuming $P_{H2} = 1$ bar and $T = 25$ °C to simplify the condition, are shown below, where $E°$ is the standard reduction potential, E_e is the equilibrium reduction potential under non-standard conditions and SHE represents the standard hydrogen electrode. In these equations and the following discussion, we used concentrations instead of activities for the sake of notational simplicity as the distinction between them does not affect the discussion in this work.

Acidic condition (pH 0)

$$2H_3O^+ + 2e^- \rightarrow H_2 + 2H_2O \quad E° = 0.000\ \text{V versus SHE} \tag{1}$$

Nernst equation

$$E_e = E° - 0.059\ \text{V}\ \log \frac{1}{[H_3O^+]}$$
$$E_e = 0.000\ \text{V} - 0.059\ \text{V} \times \text{pH} \tag{2}$$

Basic condition (pH 14)

$$2H_2O + 2e^- \rightarrow H_2 + 2OH^- \quad E° = -0.827\ \text{V versus SHE} \tag{3}$$

Nernst equation

$$E_e = E° - 0.059\ \text{V}\ \log[OH^-]$$
$$E_e = -0.827\ \text{V} + 0.059\ \text{V} \times \text{pOH} \tag{4}$$

The standard conditions are those in which the activities of all reactants and products are unity. Because equation (1) contains H_3O^+ as the reactant, the pH of the standard conditions for the reaction written in equation (1) is 0; and because equation (3) contains OH^- as one of the products, the pH of the standard conditions for the reaction written in equation (3) is 14. While equation (1) uses H_3O^+ as the reactant and equation (3) uses H_2O as the reactant, they describe the same HER reaction. Thus, at any given pH, the thermodynamic equilibrium potential for H_3O^+ reduction calculated using equation (2) and that for H_2O reduction calculated using equation (4) are always identical. What is unique about the HER compared to other redox reactions is that when the same reaction is written under acidic versus basic conditions, the redox-active species in the acidic condition (H_3O^+) is transformed to the solvent (H_2O). This raises a few interesting questions. Are H_3O^+ and H_2O then interchangeable species when considering the HER? Or are they different species that just have the same reduction potential? If H_3O^+ and H_2O have the same reduction potential and H_2O is also the solvent, should one expect not to see a diffusion-limited current for the HER even when the HER is performed under mild pH conditions with limited H_3O^+ concentrations?

These questions are not of concern when the HER is performed in a strongly acidic or basic condition. In a strongly acidic solution where H_3O^+ is abundant, considering only H_3O^+ reduction is sufficient to understand the HER. In a strongly basic condition where the concentration of H_3O^+ is negligible, considering only H_2O reduction is sufficient to understand the HER. However, for the HER under mild pH conditions where the concentration of H_3O^+ is neither abundant nor negligible, understanding the relationship between H_3O^+ reduction and H_2O reduction is critical to accurately interpret and predict the current–potential (*J*–*V*) profiles of the HER.

In an ideal case where both H_3O^+ and H_2O reduction, and water dissociation and acid–base neutralization are extremely fast under all conditions, equations (1) and (3) are indistinguishable. In this case where both the H_3O^+ and H_2O reduction are under thermodynamic control, the Nernst equation is sufficient to understand the behaviour of the HER. However, in reality, H_3O^+ and H_2O reduction are not under thermodynamic control under all conditions. In such a case, the HER behaviour of H_3O^+ and H_2O should be discussed separately and will depend on their individual kinetics, which are not identical. The various cases created by different H_3O^+ and H_2O reduction kinetics have not been comprehensively or explicitly discussed in previous studies. Below, we provide experimental data and discussions critical to gain a conceptual and coherent understanding of H_3O^+ reduction and H_2O reduction under mild pH conditions.

HER in mild pH solutions

Figure 1a shows schematically drawn linear sweep voltammograms (LSVs) of the HER in unbuffered and unstirred solutions with pH 0, 1, 7 and 12 at 25 °C with 1 bar of H_2 pressure under two assumptions. First, as H_3O^+ and H_2O have the same reduction potential and H_2O is the solvent, the mass-transport limitation of H_3O^+ should not limit the current. Second, the kinetics of H_3O^+ and H_2O reduction on the electrode are fast with no overpotential required to induce the HER current at the expected thermodynamic equilibrium potential at each pH. As a result, the reduction onset potential shifts by −59 mV pH^{-1} as predicted by equations (2) and (4).

When we experimentally obtain LSVs with a platinum working electrode (WE) in unbuffered and unstirred solutions saturated with H_2 at pH 0, 1, 7 and 12 (Fig. 1b), they look quite different from those shown in Fig. 1a except for the case with pH 0, the strongly acidic condition. At pH 1 two reduction features are observed. The onset of the first feature (marked as 1) occurs at around −0.059 V_{SHE}, which is the equilibrium potential for H_3O^+ and H_2O reduction at pH 1 using equations (2) and (4). However, this reduction feature shows a diffusion-limited behaviour. The second reduction feature (marked as 2) appears at around −0.8 V_{SHE}, and does not show a diffusion-limited behaviour. At pH 7 appreciable reduction current does not appear until around −0.7 V_{SHE}, which is considerably more negative than the expected onset potential (−0.413 V_{SHE}). At pH 12, the reduction current also appears at around −0.7 V_{SHE} but this is the expected equilibrium potential for H_3O^+ and H_2O reduction at pH 12. The discrepancy between Fig. 1a and Fig. 1b clearly demonstrates that the assumptions made to generate Fig. 1a do not hold and cannot be used to accurately predict the HER behaviour under mild pH conditions.

The most intuitive and perhaps most widely believed explanation for the two reduction features shown at pH 1 is that the kinetics of H_3O^+ reduction and H_2O reduction are different; platinum is more catalytic for H_3O^+ reduction than H_2O reduction, and the kinetics of H_2O reduction in general is much slower than that of H_3O^+ reduction[12–21]. As a result, despite their thermodynamic reduction potentials being the same, H_3O^+ reduction occurs at the thermodynamic reduction potential but H_2O reduction on platinum is considerably delayed in

https://doi.org/10.1038/s41929-025-01339-0

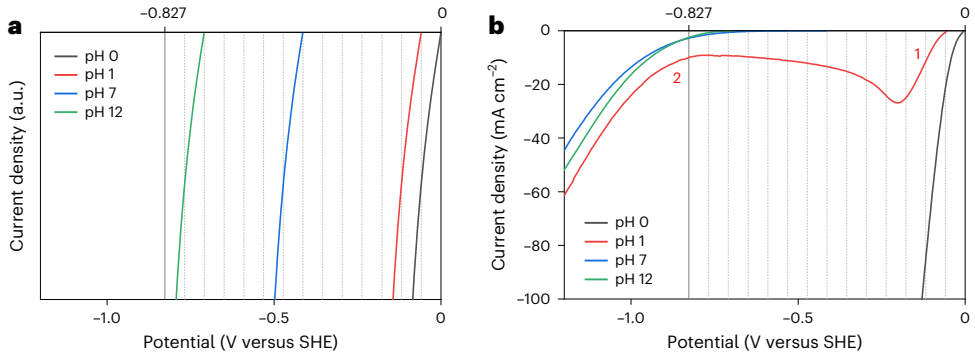

Fig. 1 | Expected and observed LSVs for the HER. a, Schematic LSVs for the HER in unbuffered, unstirred solutions of pH 0, 1, 7 and 12, assuming the HER onset occurs at the thermodynamic equilibrium potentials. **b**, LSVs experimentally collected using a platinum electrode as the working electrode in unbuffered, unstirred solutions of pH 0, 1, 7 and 12 saturated with H_2 and with sufficient supporting electrolyte (scan rate, 50 mV s^{-1}). The background grids are spaced by 59 mV between 0.000 V_{SHE} and −0.827 V_{SHE}.

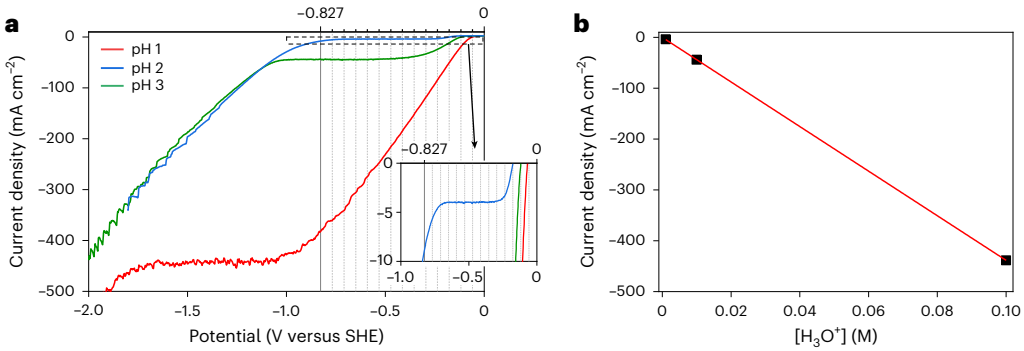

Fig. 2 | Results from unbuffered pH 1–3 solutions with convection. a, LSVs collected using a platinum RDE in unbuffered 1 M $NaClO_4$ solutions saturated with H_2 at pH 1–3 (rotation speed, 3,000 rpm; scan rate, 50 mV s^{-1}). **b**, Plot showing J_L as a function of $[H_3O^+]$ in solution.

the negative direction. Although this explanation can explain the LSV at pH 1, it cannot explain the LSV at pH 12. At pH 12, since the concentration of H_3O^+ is negligible, the first and only reduction feature appearing at −0.7 V_{SHE} should be due to H_2O reduction. However, −0.7 V_{SHE} is the thermodynamic equilibrium potential for H_2O reduction (−0.706 V_{SHE}). This means that H_2O reduction whose onset in a pH 1 solution is considerably delayed due to kinetic issues has no problem appearing at the thermodynamic reduction potential at pH 12. Does this mean that pH can drastically affect the overpotential required for the onset of H_2O reduction?

Before answering these questions, let us first confirm that the first reduction feature at pH 1 in Fig. 1b is truly due to the mass-transport limitation of H_3O^+. To confirm this, we collected LSVs using a platinum rotating disk electrode (RDE) at pH 1, 2 and 3 (Fig. 2a). As the rotation of the RDE introduces convection as a means of mass transport, the feature that previously showed as a diffusion-limited reduction peak now appears as a plateau, which is called a limiting current (J_L). The J_L is proportional to the concentration of the reactant in the bulk solution (that is, the bulk H_3O^+ concentration). When the J_L is plotted against the H_3O^+ concentration in the bulk solution, we get a straight line, meaning the reduction rate has a first-order relationship with the concentration of H_3O^+ in the solution (Fig. 2b). This confirms that the feature marked as 1 in Fig. 1b is truly due to the diffusion limitation of H_3O^+. However, although this first reduction feature is limited by H_3O^+ diffusion, this does not automatically mean that the first reduction feature is only due to H_3O^+ reduction. This is because if H_2O reduction is fast enough to establish the equilibrium pH on the electrode surface (that is, under thermodynamic control), H_2O reduction would also create a current plateau region limited by H_3O^+ diffusion (see Supplementary Note 1 for details), making contributions from the H_3O^+ reduction and H_2O reduction indistinguishable[22].

Indeed, the most systematic way to discuss the HER under mild pH conditions is to discuss three different cases depending on the individual H_3O^+ and H_2O reduction kinetics. Case 1 is when both H_3O^+ reduction and H_2O reduction are extremely fast, making the HER under thermodynamic control under all conditions. In this case, H_3O^+ reduction and H_2O reduction are not distinguishable and the equilibrium pH at the electrode surface is maintained under all conditions. However, case 1 does not exist in reality as evidenced by many previous papers showing that the kinetics of H_2O reduction are much slower than those of H_3O^+ reduction even on platinum, the best HER catalyst[12,13,15–19,23]. Case 2 is when either H_3O^+ reduction or H_2O reduction (not both) is fast enough to make the HER be under thermodynamic control under all conditions. In this case, H_3O^+ reduction and H_2O reduction are distinguishable, but the equilibrium pH predicted by the Nernst equation is still maintained at the electrode surface under all conditions. Case 3 is when neither H_3O^+ reduction nor H_2O reduction is fast enough to make the HER be under thermodynamic control under some or all conditions. In this case, H_3O^+ reduction and H_2O reduction are distinguishable and the equilibrium pH at the electrode surface is not maintained under some or all conditions.

In this study, we will discuss case 2 and case 3 in detail where H_3O^+ reduction and H_2O reduction are distinguishable (that is, the first reduction feature is for H_3O^+ reduction and the second reduction feature is for H_2O reduction when two HER features appear). Case 1, which does not distinguish H_3O^+ reduction and H_2O reduction and was covered in detail by a previous study[22], is briefly described in Supplementary Note 1 to contrast to case 2. We first discuss the behaviour on platinum

(which has often been described as being case 1) as case 2, and we show further that the behaviour on platinum may even deviate from case 2 to case 3 under some conditions. Then, we discuss the behaviours of gold, copper, silver and indium in case 3 to show the generality of case 3.

H_3O^+ reduction and H_2O reduction on platinum

Now we discuss why the H_2O reduction onset in a pH 12 solution occurs at the thermodynamic H_2O reduction potential while it is delayed at pH 1 on platinum (Fig. 1b). The rate of H_2O reduction is shown in equation (5), where $[H_2O]_s$ represents the H_2O concentration at the electrode surface and a is the reaction order.

$$\text{rate of } H_2O \text{ reduction} = k[H_2O]_s^a \tag{5}$$

The rate constant k is composed of $k°$, the standard rate constant, which varies with the HER mechanisms and the catalyst types, and an exponential function of the applied potential (E_{appl}) (equation (6)), where $E°_{H_2O}$ is the standard reduction potential of H_2O shown in equation (3) (−0.827 V_{SHE}), α_{H_2O} is the charge-transfer coefficient, n is the number of electrons involved in the electrode reaction, F is the Faraday constant, R is the ideal gas constant and T is the temperature (in kelvin).

$$k_{H_2O} = k°_{H_2O} \exp\left[-\alpha_{H_2O} nF\left(E_{appl} - E°_{H_2O}\right)/RT\right] \tag{6}$$

The rate and rate constant for H_3O^+ reduction are also shown in equations (7) and (8), where b is the reaction order and $E°_{H_3O^+}$ is the standard reduction potential of H_3O^+ shown in equation (1) (0.000 V_{SHE}).

$$\text{rate of } H_3O^+ \text{ reduction} = k[H_3O^+]_s^b \tag{7}$$

$$k_{H_3O^+} = k°_{H_3O^+} \exp\left[-\alpha_{H_3O^+} nF\left(E_{appl} - E°_{H_3O^+}\right)/RT\right] \tag{8}$$

Equations (6) and (8) show that both k_{H_2O} and $k_{H_3O^+}$ increase exponentially when E_{appl} is shifted to the negative direction, but their $E°$ values are different. The thermodynamic HER onset potential at pH 1 is −0.059 V_{SHE}. This value is more negative than and close to $E°$ for H_3O^+ reduction but it is more positive than and far away from $E°$ for H_2O. The exponential term in equation (6) is thus considerably smaller than that in equation (8). Furthermore, $k°_{H_3O^+}$ is also known to be larger than $k°_{H_2O}$ based on their activation energies for both the Volmer step and Heyrovsky step because the transfer of H^+ from H_3O^+ to the electrode surface needed for the Volmer step and Heyrovsky step is much more facile than that from H_2O (refs. 16–18,21,24). With its much larger k and a sufficiently high $[H_3O^+]_s$, H_3O^+ reduction can occur at the thermodynamic HER potential in a pH 1 solution. By contrast, near the onset potential (−0.059 V_{SHE}) region, k_{H_2O} appears to be too small to induce meaningful H_2O reduction.

In a pH 12 solution, the thermodynamic HER potential is −0.708 V_{SHE}, which is much closer to the $E°$ of H_2O reduction. Thus, k_{H_2O} at −0.708 V_{SHE} is remarkably larger than that at −0.059 V_{SHE} and it is sufficiently high to induce meaningful H_2O reduction at its thermodynamic onset potential in a pH 12 solution. This means that the reason why H_2O reduction occurs at the thermodynamic H_2O reduction potential at pH 12 but not at pH 1 is not because a higher pH improves the kinetics of H_2O reduction. Rather, it is because the thermodynamic potential for H_2O reduction at pH 12 is located nearer the $E°$ for H_2O reduction, and in this more negative potential region, the H_2O reduction kinetics are considerably improved compared with those in the less negative potential region. (Note that $k_{H_3O^+}$ at −0.708 V_{SHE} would also be remarkably larger than that at −0.059 V_{SHE}. However, the surface H_3O^+ concentration at around −0.708 V_{SHE} is negligible, making the rate of H_3O^+ reduction negligible.)

This, though, prompts another set of questions. If H_2O reduction near −0.708 V_{SHE} is fast enough to induce H_2O reduction at the thermodynamic reduction potential in a pH 12 solution, why does the second reduction feature in an unstirred pH 1 solution not appear until around −0.8 V_{SHE} (Fig. 1b)?

Emergence of the second HER feature

To understand when the H_2O reduction feature appears as the second reduction feature, we collected LSVs using a platinum RDE in unbuffered solutions with pH varying from 0 to 14 (Fig. 3). LSVs obtained in acidic solutions, except for the one obtained in a strongly acidic solution (pH 0), show two reduction features. Similar to the pH 1 case discussed above, the first feature occurs at or very near the thermodynamic HER potential for the given pH. The second feature occurs at more negative potential. Before the second feature appears, the first feature shows J_L limited by the mass transport of H_3O^+.

Before we discuss the factors that affect the potential at which the second feature appears, we would like to remind readers of the following facts from basic electrochemistry and acid–base equilibria.

First, the applied potential affects the pH at the electrode surface according to the Nernst equation; when a potential is applied to the solution, the surface $[H_3O^+]$ will change in an attempt to establish the equilibrium pH corresponding to the applied potential. Equation (2) shows how the bulk solution pH affects the equilibrium reduction potential of H_3O^+. The same equation can be rearranged to show how the applied potential (E_{appl}) would affect the equilibrium pH at the electrode surface ($pH_{surface}$) during the LSV in any solution (equation (9)).

$$E_{appl} = 0.000\,\text{V} - 0.059\,\text{V} \times \text{pH}_{surface} \tag{9}$$

If the electrode kinetics are fast, the real surface pH during the LSV will be exactly the pH predicted by equation (9). If the electrode kinetics are slow, the surface pH may lag behind that predicted by the Nernst equation. Nonetheless, when a potential is applied, the system's attempt to establish a new equilibrium composition at the electrode surface drives the Faradaic reaction, generating current. For the sake of simplicity, for the description provided below we will assume that for a platinum WE the surface pH during an LSV can be predicted by equation (9) under all conditions because the kinetics of either H_3O^+ reduction or H_2O reduction are fast enough to yield the equilibrium pH (that is, case 2 mentioned above).

Second, the surface pH can be raised either by consuming H_3O^+ through H_3O^+ reduction (equation (1)) or by a neutralization reaction with OH^- generated through H_2O reduction (equation (3)).

Third, because of the logarithmic scale of pH and the autodissociation constant, K_w (1×10^{-14} at 25 °C), the change in the surface H_3O^+ concentration ($[H_3O^+]_s$) needed to increase the surface pH by 1 at low pH and the change in the surface OH^- concentration ($[OH^-]_s$) needed to increase the surface pH by 1 at high pH are considerable, whereas the change needed at mild pHs is very small (Supplementary Table 1).

We will now explain the behaviour of the LSV in acidic media using the LSV obtained at pH 3 as an example, which is separately shown in Fig. 3c. The thermodynamic potential for H_3O^+ reduction is −0.177 V_{SHE} and the H_3O^+ reduction current indeed appears at −0.177 V_{SHE}. When the potential is swept from its equilibrium potential of −0.177 V_{SHE} (surface pH 3) to −0.236 V_{SHE} (surface pH 4), the H_3O^+ reduction current keeps increasing to decrease the $[H_3O^+]_s$ from 10^{-3} M to 10^{-4} M. Alternatively, the $[H_3O^+]_s$ can also decrease from 10^{-3} M to 10^{-4} M by H_2O reduction increasing the $[OH^-]_s$ from 10^{-11} M to 10^{-10} M; as $[OH^-]_s$ increases, $[H_3O^+]$ automatically decreases via the water autodissociation equilibrium. However, the H_2O reduction kinetics in this potential region are much slower[16,18,21] and the HER current in this region is mostly governed by H_3O^+ reduction.

When the potential is further swept to −0.295 V_{SHE} (equivalent to surface pH 5), the H_3O^+ reduction current keeps increasing to increase

https://doi.org/10.1038/s41929-025-01339-0

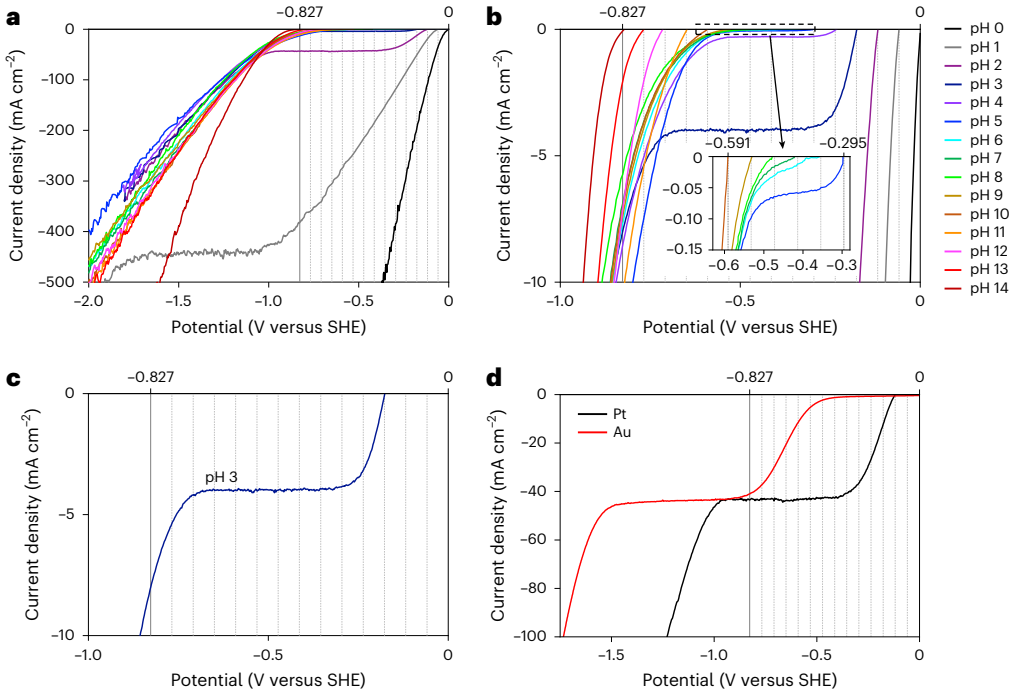

Fig. 3 | LSVs in unbuffered pH 0–14 solutions with convection. a, LSVs collected using a platinum RDE in unbuffered solutions of pH 0–14 saturated with H_2. **b**, The same LSVs showing the onset region magnified. **c**, LSV at pH 3 shown separately, **d**, LSVs at pH 2 measured with platinum and gold RDEs. For all data, the rotation speed is 3,000 rpm and the scan rate is 50 mV s^{-1}.

the surface pH to 5 while the diffusion flux of H_3O^+ from the bulk solution to the electrode keeps increasing. The diffusion flux of H_3O^+ at the electrode surface is the difference between the bulk $[H_3O^+]$ ($[H_3O^+]_{bulk}$) and $[H_3O^+]_s$ divided by the thickness of the Nernst diffusion layer (δ) (equation (10)), where δ is determined by the diffusion coefficient of H_3O^+ (D), the rotating speed of the RDE (ω) and the kinematic viscosity of the solution (ν) as shown in equation (11). (The Nernst diffusion layer is a layer where mass transport occurs only via diffusion between the electrode surface and the bulk solution under convection.) At −0.295 V_{SHE}, the equilibrium $[H_3O^+]_s$ becomes 10^{-5} M, which is negligible compared with the bulk concentration. At this point, the diffusion flux of H_3O^+ at the surface is maximized and the diffusion-limited current, which is proportional to the diffusion flux of H_3O^+, is also maximized (that is, it reaches J_L) (equations (12) and (13)).

$$\text{flux of } H_3O^+ \text{ at the surface} = D\left(\left[H_3O^+\right]_{bulk} - \left[H_3O^+\right]_s\right)/\delta \quad (10)$$

$$\delta = 1.61\nu^{1/6}D^{1/3}\omega^{-1/2} \quad (11)$$

$$J_{diffusion} = nFD\left(\left[H_3O^+\right]_{bulk} - \left[H_3O^+\right]_s\right)/\delta \quad (12)$$

$$J_L = nFD\left[H_3O^+\right]_{bulk}/\delta \quad (13)$$

Once the limiting current is achieved, applying a more negative potential does not further increase the HER current (the current plateau in Fig. 3c) until the surface pH becomes ~11. This is because the $[H_3O^+]_s$ that needs to be additionally removed to increase surface pH from 5 to 11 is negligible and applying a more negative potential would not change the flux of H_3O^+ in equation (10) notably. For example, when the potential is further swept to −0.413 V_{SHE} and the surface $[H_3O^+]_s$ is further reduced to 10^{-7} M, this makes no meaningful difference to the flux of H_3O^+ (that is, $D(10^{-3}\,M - 10^{-5}\,M)/\delta$ versus $D(10^{-3}\,M - 10^{-7}\,M)/\delta$).

While the potential is swept in the negative direction, however, k_{H_2O} gradually increases and the H_2O reduction rate eventually becomes non-negligible. (The potential at which H_2O reduction is first meaningfully enabled would depend on the catalytic ability for H_2O reduction of the specific electrode used.) When OH^- is generated as a result of H_2O reduction, it reacts with H_3O^+ diffusing toward the electrode surface in the Nernst diffusion layer, thus decreasing the net incoming H_3O^+ flux to the electrode surface. This means that the incoming H_3O^+ flux from the bulk solution can now be consumed either by H_3O^+ reduction or by a neutralization reaction with OH^- generated from H_2O reduction. (The HER current needed to establish the equilibrium surface pH is the same whether the surface pH is increased by H_3O^+ reduction or by H_2O reduction.) With an increasing rate of H_2O reduction generating more OH^- as the potential becomes more negative, the incoming H_3O^+ flux at the electrode surface keeps decreasing and eventually becomes negligible. As a result, the H_3O^+ reduction current decreases accordingly and eventually becomes negligible, making the majority of the plateau current come from H_2O reduction at these more negative potentials. (We cannot be certain about the exact potential at which the majority of the plateau current come from H_2O reduction, but we make an assumption here that it is before the second reduction feature appears).

When the potential is further swept in the negative direction, the amount of OH^- needed to increase the surface pH (or decrease surface pOH) keeps increasing (Supplementary Table 1), increasing the H_2O reduction current accordingly. In the middle potential region, the increase in $[OH^-]_s$ is negligible, meaning the flux of OH^- from the surface and thus the increase in the current above the limiting current value for H_3O^+ mass transport is also negligible. However, as $[OH^-]_s$ becomes notably higher than $[OH^-]_{bulk}$, the diffusion of surface OH^- to the bulk solution increases, requiring more HER to occur to maintain the equilibrium surface pH. Eventually, at a certain potential where the H_2O reduction current notably exceeds the plateau current, the H_2O reduction current emerges beyond the J_L as the second reduction feature.

For the LSV at pH 3, the second feature appears at around −0.69 V_{SHE} where the surface $[OH^-]_s$ should become between 10^{-3} M and 10^{-2} M. This understanding means that the potential where the second reduction feature appears is not the potential at which H_2O reduction is enabled for the first time but rather the potential at which the current for H_2O reduction surpasses the J_L that comes from the mass-transport limitation of H_3O^+.

HER in near-neutral solutions

Next, we discuss why the LSVs collected in near-neutral solutions (pH 6–9) look more or less similar in Fig. 3b. As mentioned above, varying the surface pH in the middle pH region requires very little change in $[H_3O^+]_s$ and $[OH^-]_s$ (Supplementary Table 1) and also does not result in much flux of OH^- from the electrode surface nor H_3O^+ to the surface. Thus, the HER current near the onset region of LSVs obtained in pH 6–8 solutions remains low until the applied potential reaches about −0.55 V_{SHE} (surface pH ~9) where further increasing the surface pH requires considerable OH^- generation.

In solutions with pH 9 and above, appreciable H_2O reduction occurs at the onset potential because increasing the surface pH from 9 requires considerable H_2O reduction. As the HER onset in pH 9 is −0.55 V_{SHE} and LSVs obtained in pH 6–8 solutions do not show appreciable HER current until about −0.55 V_{SHE}, those obtained in pH 6–9 will look more or less similar unless the onset region is closely magnified (Fig. 3b). With these features, one may think the HER onset in pH 6–8 solutions is delayed and conclude that the kinetics of H_2O reduction are slow in pH 6–8 solutions. However, the truth is that no matter how good a catalyst is used, the HER current near the onset potential in unbuffered pH 6–8 solutions will always be low because it is limited by the very low H_3O^+ and OH^- fluxes at the equilibrium surface pHs produced by the potentials applied near the thermodynamic onset.

We note that while the H_2O reduction kinetics on platinum in basic solutions appear to be sufficiently fast to induce an HER current at the thermodynamic onset potential, when we compare the HER current in a pH 0 solution near the onset region, which is due to H_3O^+ reduction, and the HER current in a pH 14 solution near the onset region, which is due to H_2O reduction, the overpotential required to achieve 1 mA cm^{-2} is 4.2 mV and 34.9 mV, respectively (Fig. 3b). This means that H_2O reduction kinetics are still slower than H_3O^+ reduction kinetics in strongly acidic conditions (that is, $k^\circ_{H_3O^+}$ is considerably higher than $k^\circ_{H_2O}$) as discussed in many previous papers[18,19,21,24–27]. This also means that our assumption that platinum belongs to case 2 may not be true for the potential region where the surface pH is changed mainly by H_2O reduction and the diffusion of OH^- from the electrode surface to the bulk is fast. Under this condition, platinum may fail to establish the equilibrium surface pH, meaning platinum would more properly belong to case 3.

HER on electrodes with slow HER kinetics

For electrodes with slower HER kinetics than platinum, all the basic reduction features will appear in the same manner, but they will shift in the negative direction because a greater overpotential is needed to achieve the same level of HER current than is needed on platinum. Also, when the potential is swept in the negative direction, the surface pH cannot be predicted by the Nernst equation and will always be lower than the thermodynamically predicted surface pH. This can be best demonstrated by gold, which is an extreme example of case 3 in that the kinetics of both H_2O and H_3O^+ reduction on gold are too slow to establish the equilibrium pH at all potentials. In case 3, the degree of shift of the reduction features or the deviation of the surface pH from the equilibrium pH will depend on the HER kinetics of the electrode used and the reaction conditions.

Figure 3d shows a comparison of LSVs in a pH 2 unbuffered solution obtained with platinum and gold using the same RDE set-up. On gold with slow HER kinetics, while the H_3O^+ reduction still occurred at the thermodynamic onset potential, the H_3O^+ reduction current increases much more slowly with the potential sweep, meaning the equilibrium surface pH is not established at potentials in this region. In addition, the plateau current on gold is achieved at a more negative potential (by >500 mV) than on platinum, meaning a more negative potential must be applied to deplete H_3O^+ at the electrode surface. This clearly shows that the HER on gold is under kinetic control. This makes the assignments of the two reduction features more straightforward for the case of gold.

When the HER is under thermodynamic control (that is, the surface pH is in equilibrium with the applied potential), a current plateau in the middle potential region (surface pH 4–10) with J_L determined by H_3O^+ diffusion will be observed in mildly acidic solutions even if H_2O, which is the solvent and therefore abundant, is being reduced. This is because no matter how good the catalyst, the surface pH cannot be made more basic than the equilibrium pH for the applied potential, meaning the maximum achievable current is given by the flux of H_3O^+ to the surface and OH^- from the surface at this equilibrium pH. At the surface pHs corresponding to these applied potentials, the OH^- flux is negligible and the H_3O^+ flux is essentially constant, as its surface concentration is already very low and does not change much in absolute terms as the pH becomes more basic. This means that any HER catalyst good enough to be under thermodynamic control will show the same mass-transport-limited current plateau regardless of how good it is at doing H_2O reduction.

By contrast, when the HER is under kinetic control, such as is the case for gold (and other electrocatalysts with poorer catalytic ability than platinum), the presence of the mass-transport-limited plateau alone is enough to assign the first feature to H_3O^+ reduction because H_2O reduction not under thermodynamic control has no way to generate a plateau limited by H_3O^+ diffusion. As the potential is swept in the negative direction, the rate constant for H_2O reduction, k_{H_2O}, will increase exponentially (equation (6)). As the reaction is not under thermodynamic control and the reactant, H_2O, is the solvent and thus cannot experience meaningful mass-transport limitation, if H_2O reduction were occurring to an appreciable extent in this potential region, we would observe an exponential increase in the reduction current to match the exponential rise in k_{H_2O}. Thus, the presence of a plateau current means k_{H_2O} is still too small in this potential region for H_2O reduction to meaningfully contribute to the current. Instead, the HER current in the plateau region is due to H_3O^+ reduction, which is kinetically more facile (that is, $k_{H_3O^+} \gg k_{H_2O}$) and which will experience mass-transport limitation at the observed J_L even when the HER is not under thermodynamic control. Eventually, as the applied potential is swept to sufficiently negative values, k_{H_2O} increases to the point where H_2O reduction becomes substantial. This allows the H_2O reduction current to exceed the J_L for H_3O^+ diffusion and causes the second reductive wave to emerge.

We note that the difference in the overpotential required to induce substantial H_2O reduction versus H_3O^+ reduction is catalyst dependent, because each catalyst has different kinetics for H_3O^+ reduction and H_2O reduction. This point is well demonstrated by LSVs obtained with copper, silver and indium electrodes, which are frequently used in various reduction reactions in aqueous media such as CO_2 reduction and nitrate reduction[28–31], in a pH 2 solution that is unstirred so the onset of the second HER feature is easier to resolve (Fig. 4). All metals show two HER features in this mildly acidic solution. Like gold, all of these metals are poor HER catalysts, which is confirmed by their first HER onsets appearing at much more negative potentials than the thermodynamic equilibrium HER potential (−0.118 V versus SHE at pH 2). In this case where the HER is clearly not under thermodynamic control, and therefore the HER current is not regulated by establishing the equilibrium surface pH, H_2O reduction has no reason to show diffusion-limited current. Thus, the two HER features can be straightforwardly assigned; the first HER feature showing diffusion-limited behaviour is due to H_3O^+ reduction (as H_3O^+), and the second HER feature not showing diffusion-limited

https://doi.org/10.1038/s41929-025-01339-0

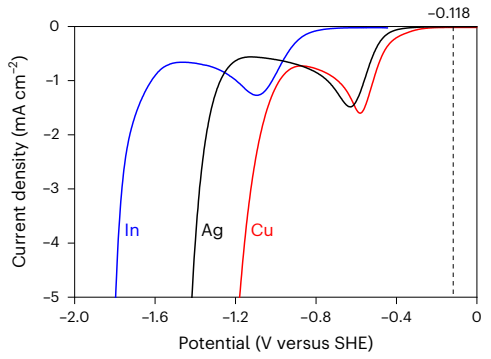

Fig. 4 | LSVs of poor HER catalysts in an unbuffered, unstirred pH 2 solution. LSVs of copper, silver and indium in an unbuffered, unstirred pH 2 solution saturated with H_2 and containing sufficient supporting electrolytes (scan rate, 50 mV s^{-1}). The dashed line represents the thermodynamic equilibrium HER potential at pH 2 (−0.118 V_{SHE}).

behaviour is due to H_2O reduction. These metals show different onsets for both H_3O^+ reduction and H_2O reduction. In addition, the distance between the H_3O^+ reduction onset and the H_2O reduction onset is metal dependent. For example, while copper and silver show similar onsets for H_3O^+ reduction, their onsets for the H_2O reduction features are quite different. This confirms that each metal has different kinetics for H_3O^+ reduction and H_2O reduction and that these differences determine where the reduction onsets for the two features occur.

HER in buffered solutions

The above analysis dealt exclusively with unbuffered solutions; however, it is also important to understand how the presence of a buffer affects LSVs obtained at various pHs. We collected LSVs in buffered solutions ranging from pH 0 to 14 using the same RDE set-up described above with platinum. As there is no single buffer available with a working range that spans from 0 to 14 we varied the buffer based on the pH we wished to maintain. Experimental details can be found in the Methods. The results are shown in Fig. 5a,b.

In unbuffered solutions, the systematic shift of the HER reduction onset was not obvious in the middle pH solutions owing to how easy it is to increase the surface pH in their onset region. In buffered solutions, an appreciable HER current is observed in the onset region even in the middle pH solutions. This is because the conjugate acid of the buffer serves as a proton donor and keeps releasing protons, requiring more HER current to increase the surface pH. To increase pH in the buffered solution, the conjugate base (A^-) to conjugate acid (HA) ratio([A^-]/[HA]) must change by consuming a sufficient amount of the conjugate acid, as shown in the Henderson–Hasselbalch equation.

$$\mathrm{pH} = \mathrm{p}K_a + \log_{10}\left(\frac{[\mathrm{A}^-]}{[\mathrm{HA}]}\right) \tag{14}$$

For example, in a pH 6 unbuffered solution, increasing the surface pH from 6 to 7 requires changing $[H_3O^+]_s$ from 10^{-6} M to 10^{-7} M by H_3O^+ reduction, which is not much and does not cause much flux. However, in a pH 6 solution buffered with 0.5 M phosphate (at pH 6, $[H_2PO_4^-]$:$[HPO_4^{2-}]$ = 15.8:1, meaning $[H_2PO_4^-]$ is 0.47 M using 7.2 as the pK_{a2} of H_3PO_4), H_3O^+ reduction must occur until $[H_2PO_4^-]_s$ is lowered from 0.47 M to 0.27 M to increase the surface pH from 6 to 7. This requires considerable HER to occur to raise the pH and to maintain that pH despite a considerable flux of $H_2PO_4^-$ to the surface and HPO_4^{2-} from the surface.

We note that it may be possible that the conjugate acid donates a proton directly to the electrode surface, instead of donating a proton to H_2O to form H_3O^+, which then can donate a proton to the electrode[32–34]. The former could be distinguished as conjugate acid reduction rather than H_3O^+ reduction; however, in our discussion focusing on the difference between H_3O^+ reduction and H_2O reduction, we include the conjugate acid reduction within H_3O^+ reduction as they will appear as the same reduction feature.

In buffered solutions, while the conjugate acid of the buffer serves as an additional proton source and alleviates the mass-transport limitation of H_3O^+, the conjugate acid can also be eventually depleted at the electrode surface. Thus, mass-transport-limited current can still be observed in buffer solutions, and it is now due to the mass-transport limitation of the conjugate acid as well as H_3O^+. This is well demonstrated in Fig. 5c which compares LSVs obtained in unbuffered and buffered pH 3 solutions; J_L is higher in the buffered solution because J_L in the buffered solution is determined by the flux of HSO_4^- and H_3O^+.

Furthermore, even for solutions with the same pH and overall buffer concentration, the limiting current behaviour can be different if they have different concentrations for the conjugate acid specifically. For example, Fig. 5d compares LSVs obtained in pH 6 acetate buffer versus pH 6 phosphate buffer. While these two solutions have the same pH and total buffer concentration (0.5 M), owing to their difference in pK_a, the conjugate acid concentrations in these solutions are different (0.03 M CH_3COOH in the acetate buffer and 0.47 M $H_2PO_4^-$ in the phosphate buffer, respectively.) As a result, the J_L obtained in the acetate buffer solution is lower.

In pH 3–8 buffered solutions, after the mass-transport-limited plateau current, the second reduction feature appears as was also the case in unbuffered solutions. This feature emerges at a potential where the H_2O reduction current exceeds the plateau current.

OER in acidic, basic and neutral conditions

As with the HER, the OER can be written as occurring in either acidic (equation (15)) or basic (equation (17)) conditions with the former involving H_2O oxidation and the latter involving OH^- oxidation. Their corresponding Nernst equations with P_{O_2} = 1 bar and T = 25 °C are shown in equations (16) and (18), respectively. Just like with the HER, there is only one equilibrium potential for H_2O oxidation and OH^- oxidation at any given pH.

Acidic condition (pH 0)

$$6H_2O \rightarrow O_2 + 4H_3O^+ + 4e^- \qquad E^\circ = 1.229\ \mathrm{V\ versus\ SHE} \tag{15}$$

Nernst equation

$$E_e = E^\circ - 0.059\ \mathrm{V}\ \log\frac{1}{[H_3O^+]}$$
$$E_e = 1.229\ \mathrm{V} - 0.059\ \mathrm{V} \times \mathrm{pH} \tag{16}$$

Basic condition (pH 14)

$$4OH^- \rightarrow O_2 + 2H_2O + 4e^- \qquad E^\circ = 0.403\ \mathrm{V\ versus\ SHE} \tag{17}$$

Nernst equation

$$E_e = E^\circ - 0.059\ \mathrm{V}\ \log[OH^-]$$
$$E_e = 0.403\ \mathrm{V} + 0.059\ \mathrm{V} \times \mathrm{pOH} \tag{18}$$

Given the results showing two reduction features for the HER in slightly acidic solutions (Fig. 2a), we were curious if similar behaviours would be observed for OH^- oxidation and H_2O oxidation in slightly basic solutions. As an initial test to see if this occurs, we used NiOOH, a compound that has received a great deal of attention as a water oxidation catalyst[35], as the working electrode and performed OER in an unbuffered, rapidly stirred pH 12 solution.

As can be seen in Fig. 6a, following the peak at 0.75 V_{SHE} corresponding to oxidation of $Ni(OH)_2$ to NiOOH, the LSV clearly shows the same

https://doi.org/10.1038/s41929-025-01339-0

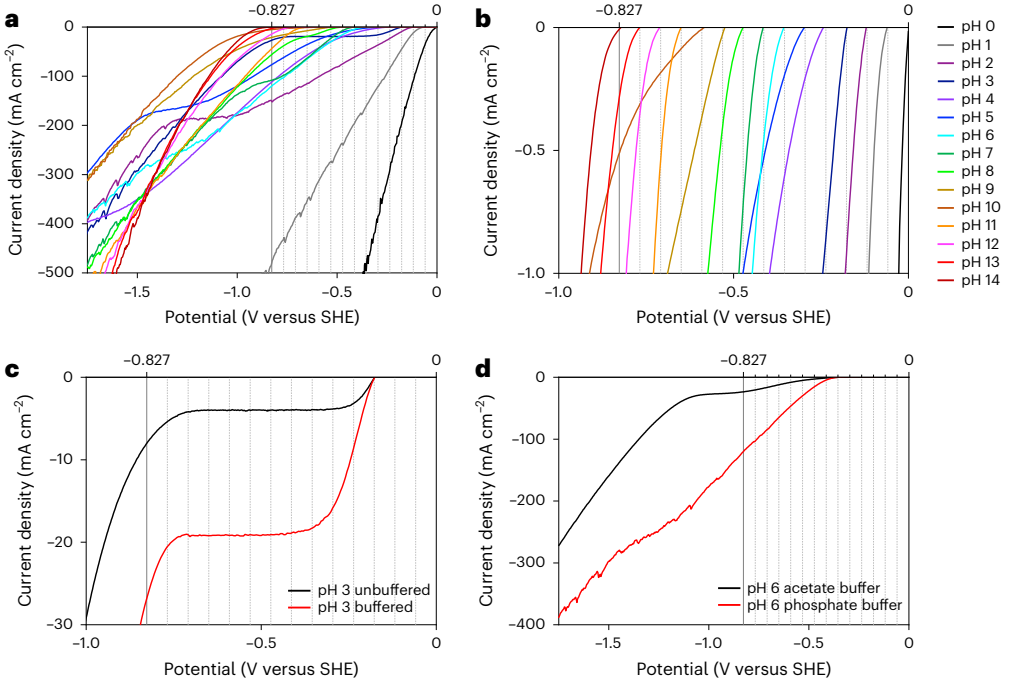

Fig. 5 | LSVs in buffered solutions with convection. a, LSVs collected using a platinum RDE in buffered solutions of pH 0–14 saturated with H_2 (rotation speed, 3,000 rpm; scan rate, 50 mV s^{-1}). **b**, The same LSVs showing the onset region magnified. **c**, LSVs in pH 3 unbuffered and buffered solutions. **d**, LSVs in pH 6 acetate and phosphate buffer solutions.

two-feature pattern: the first feature initiates at a less positive potential, followed by a mass-transport-limited plateau, while the second feature emerges above the plateau current at a more positive potential. We note that, unlike with HER on platinum, in this case the current onset is markedly delayed relative to its thermodynamic potential (by ~0.37 V), indicating that the kinetics of the OER on NiOOH are considerably poorer than those of the HER on platinum. As a consequence, the surface pH will not be in equilibrium for the applied potential and the surface pH will be substantially more basic than that predicted by the Nernst equation. This in turn makes the assignment of the two oxidation features more straightforward as in the case of assigning the two HER features on gold and other electrodes that belong to case 3; as the OER current is under kinetic control, a mass-transport-limited current plateau would not appear if H_2O oxidation oxidizing abundant solvent molecules occurs appreciably. Thus, the first oxidation feature that shows diffusion-limited behaviour must be due to OH^- oxidation and the second oxidation feature that does not show a diffusion-limited behaviour must be due to H_2O oxidation. This means that the kinetics of OH^- oxidation are faster than those of H_2O oxidation and therefore that H_2O oxidation requires more overpotential to occur.

A more comprehensive understanding of pH-dependent OER behaviours can be obtained by examining LSVs for the OER obtained in pH 0–14 solutions both unbuffered and buffered while bubbling O_2 (Fig. 6b,c). Because NiOOH is unstable in acidic media, the LSVs were collected using RuO_2 drop-cast with a C65 support onto a gold RDE electrode as the working electrode.

The results for the unbuffered solutions (Fig. 6b) closely parallel those obtained for the HER in unbuffered solutions. The OH^- oxidation appears as a single wave in highly alkaline conditions such as pH 14 and 13 because the OH^- concentration is sufficient not to cause OH^- oxidation to be mass transport limited under those conditions. In mildly alkaline conditions such as pH 12 and 11, there is a plateau caused by OH^- oxidation being mass transport limited, followed by H_2O oxidation appearing as the second oxidation feature. In pH 14–11 solutions, the OER onset shows a pH-dependent shift but the position of the onset and the degree of shift do not perfectly follow the thermodynamic prediction due to generally slow OER kinetics. Even in a pH 14 solution, the OH^- oxidation onset is delayed by 0.24 V from its thermodynamic value.

In the middle pH region (10–4), the OER onset appears not to be pH dependent. This is because in these solutions, changing the surface pH near the onset does not require much OH^- or H_2O oxidation to occur and therefore the OER current at and around the onset region is negligible. The OER current becomes appreciable when the surface pH needs to be decreased below 4. Thus, the LSVs obtained in pH 10–4 solutions show similar onsets to that in a pH 4 solution.

Supplementary Table 2 shows the equilibrium $[H_3O^+]_s$ and $[OH^-]_s$ and the surface pH and pOH when the potential is swept from 0.403 V_{SHE} to 1.229 V_{SHE}. This table makes it easy to see how much OH^- must be consumed or H_3O^+ generated to decrease the equilibrium surface pH by 1. However, it should be noted that as the OER kinetics are not fast, the actual surface pH at each potential will be higher than the equilibrium pH.

In acidic solutions (pH < 4), the OER current near the onset region is mainly from H_2O oxidation because the OH^- concentration is negligible (Fig. 6b). As decreasing the surface pH below 4 requires substantial H_3O^+ production, appreciable H_2O oxidation current is observed at the onset in these acidic solutions and therefore the onsets in these solutions clearly look pH dependent. We note again that even in the most acidic solutions the onset of H_2O oxidation does not occur until approximately 200 mV of overpotential is applied owing to the slow OER kinetics.

The data obtained for buffered solutions are shown in Fig. 6c. The addition of the buffer did not change LSV features in the strongly basic (pH 14 and 13) or strongly acidic solutions (pH 3–0). However, in pH 12–11 solutions, the mass-transport-limited feature for OH^- oxidation disappears because the conjugate base of the buffer replenishes OH^- by reacting with H_2O and prevents the depletion of OH^- at the electrode surface. The conjugate base can eventually be depleted, resulting in a mass-transport-limited current, but its depletion did not occur under the conditions used in our experiment because the OER current density was much lower than that observed for the HER.

https://doi.org/10.1038/s41929-025-01339-0

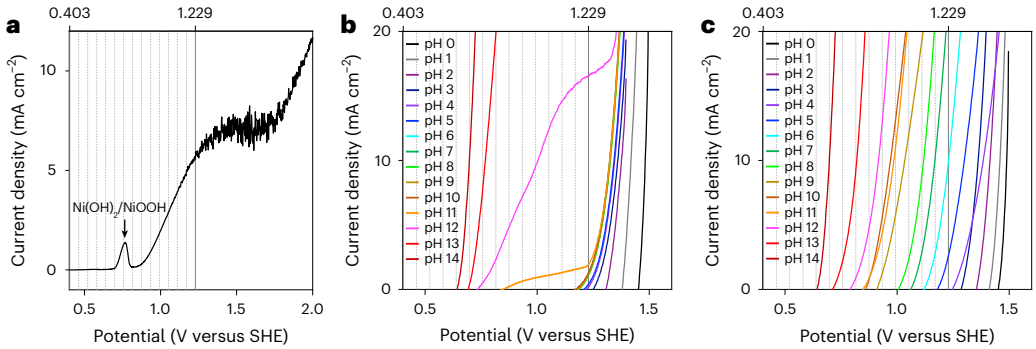

Fig. 6 | LSVs collected for the OER. a, LSV in a rapidly stirred, unbuffered 0.1 M $KClO_4$ solution (pH 12) using a $Ni(OH)_2$ working electrode (scan rate, 10 mV s^{-1}). **b**,**c**, LSVs collected using a RuO_2 RDE in unbuffered (**b**) and buffered (**c**) solutions of pH 0–14 saturated with O_2 (rotation speed, 3,000 rpm; scan rate, 50 mV s^{-1}). The background grids are spaced by 59 mV between 0.403 V_{SHE} and 1.229 V_{SHE}.

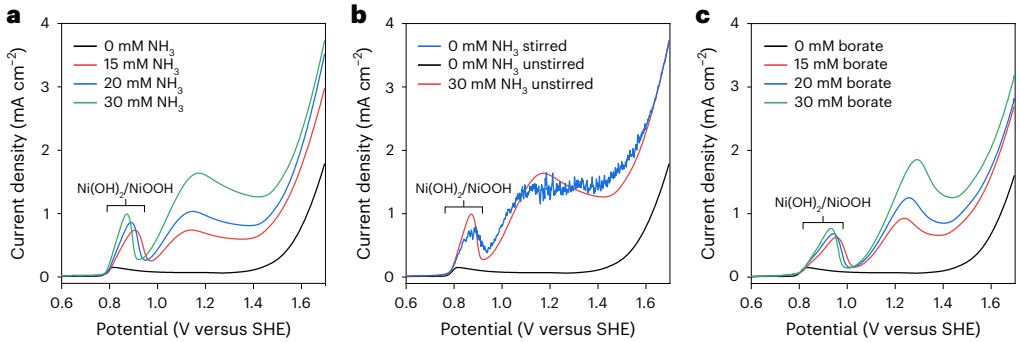

Fig. 7 | LSVs for ammonia oxidation. a, LSVs obtained in 0.5 M K_2SO_4 (pH 11) solutions containing 0–30 mM ammonium sulfate. **b**, LSV obtained in a 0.5 M K_2SO_4 (pH 11) solution with no ammonia while stirring. LSVs obtained with and without 30 mM ammonium sulfate in unstirred solutions are overlaid for comparison. **c**, LSVs obtained in 0.5 M K_2SO_4 (pH 11) solutions with 0–30 mM borate.

(Mass-transport-limited behaviours will be observed if the buffer concentration is lower or if the solution is not stirred.) Unlike in unbuffered solutions, in buffered solutions with pH 10–4, the onset clearly changes with pH because the presence of buffer resists the change of the surface pH, requiring the generation of appreciable OER current at the onset to change the surface pH. The observed potential-dependent shift of the onset, however, is not strictly −59 mV pH^{-1} because the onset potential is kinetically governed and the type of buffer used can affect the kinetics of the OER.

Ammonia oxidation as a case study

As a case study highlighting how understanding HER and OER behaviours in mild pH conditions can be important for accurate data interpretation in other aqueous reactions, we discuss ammonia oxidation on NiOOH electrodes. Several papers have investigated this material as an electrocatalyst for achieving ammonia oxidation either for potential use in a fuel cell or as a way of achieving wastewater remediation[36–40]. To gauge the activity of NiOOH toward this reaction, it has been common to compare an LSV collected in a (generally unbuffered) solution of a given pH with and without ammonia present.

Figure 7a shows LSVs obtained with and without ammonia in an unbuffered, unstirred pH 11 solution. The LSV without ammonia shows two oxidation features: the first is the oxidation peak at around 0.8 V for the oxidation of $Ni(OH)_2$ to NiOOH, and the second is the oxidation wave for water oxidation initiating at around 1.35 V_{SHE}. Note that the feature for OH^- oxidation is absent here because the amount of OH^- at the electrode surface in an unstirred, unbuffered pH 11 solution is negligible. When ammonia is added (10–30 mM), the peak for oxidation of $Ni(OH)_2$ to NiOOH increases considerably. The oxidation of $Ni(OH)_2$ to NiOOH consumes OH^- (equation (19)) and its oxidation is suppressed in an unbuffered, weakly basic solution. (The local pH decrease can even result in a dissolution loss of $Ni(OH)_2$, which can further decrease the size of this oxidation peak in unbuffered solutions.) However, ammonia serves as a weak base (accepting H^+ released from $Ni(OH)_2$ oxidation) and buffers the solution, preventing the depletion of OH^- at the electrode surface and dissolution of $Ni(OH)_2$. This enhances the peak for $Ni(OH)_2$ oxidation to NiOOH.

$$Ni(OH)_2 + OH^- \rightarrow NiOOH + H_2O + e^- \quad (19)$$

Another, even more notable feature caused by ammonia addition is the emergence of a new oxidation peak between the peak for $Ni(OH)_2$ oxidation and the wave for H_2O oxidation. The size of this new peak increases with the concentration of ammonia. Seeing this, many researchers have reached the intuitive conclusion that this new peak centred at around 1.15 V_{SHE} is due to oxidation of ammonia. However, knowledge of the kinetic differences between OH^- and H_2O oxidation and the effect of a buffer on enhancing OH^- oxidation, and the recognition that ammonia is the conjugate base of the NH_4^+/NH_3 buffer, suggests a different interpretation for the middle peak: ammonia replenishes OH^- at the electrode surface, allowing for the generation of appreciable OH^- oxidation current before H_2O oxidation initiates. As the ammonia concentration increases, the OH^- flux to the electrode increases thereby enhancing the diffusion-limited OH^- oxidation current.

To confirm that the newly appearing oxidation feature between $Ni(OH)_2$ oxidation and H_2O oxidation upon ammonia addition is due to OH^- oxidation, we performed two experiments. First, we obtained an LSV in a pH 11 solution without ammonia while stirring. Stirring increases OH^- flux to the electrode surface, which enhances OH^- oxidation. As a result, an OH^- oxidation feature appears between the $Ni(OH)_2$ oxidation and H_2O oxidation features (Fig. 7b). Note that the onset of

the newly appearing OH^- oxidation feature is identical to the onset of the middle peak observed in the presence of ammonia.

Second, we obtained LSVs in an unbuffered, unstirred pH 11 solution with 10–30 mM borate instead of 10–30 mM ammonia. Boric acid and ammonium ion have similar pK_as, meaning ammonia and borate have comparable basicity and thus are comparably good at replenishing OH^-. The LSVs obtained with borate (Fig. 7c) show middle oxidation peaks that look similar to those obtained with ammonia (Fig. 7a). These two experiments prove that the middle oxidation feature in the LSVs obtained with ammonia is not actually due to ammonia oxidation.

Previous studies examining NiOOH electrodes for ammonia oxidation have shown that during extended electrolysis, ammonia concentration decreases and oxidation products increase[36–40]. Thus, it is likely that ammonia oxidation current does contribute to some extent to the oxidation currents in the LSVs in Fig. 7a. However, our experiments show that ammonia oxidation does not create its own signature oxidation feature, meaning it cannot be clearly separated from OH^- oxidation or H_2O oxidation. If the middle oxidation peak were due to ammonia oxidation, it should be possible to obtain a high Faradaic efficiency for ammonia oxidation because it is well separated from H_2O oxidation. However, previous results commonly report a low Faradaic efficiency for ammonia oxidation[38,39] and this can be understood only when it is realized that the middle oxidation feature in the LSV is primarily due to OH^- oxidation and there is no potential region where only ammonia oxidation can occur. This example clearly demonstrates why it is critical to understand the kinetic differences between H_3O^+ and H_2O reduction and OH^- and H_2O oxidation and the effect of a buffer and stirring on their behaviours for accurately interpreting experimental results and assessing the promise of a catalyst for reduction and oxidation reactions occurring in aqueous media under mild pH conditions.

Conclusions

We have provided comprehensive results and discussions explaining the effect of pH, potential, stirring, buffer and the catalytic ability of the electrode on the HER and OER under mild pH conditions. The appearance of two HER reduction features in slightly acidic solutions and two OER features in slightly basic solutions were demonstrated. When and why the two features appear was also discussed. By starting with the Nernst equations, which do not differentiate H_3O^+ reduction from H_2O reduction for the HER and OH^- oxidation from H_2O oxidation for the OER, and demonstrating and discussing features that can be explained only by kinetic differences of these reactions, this Analysis provides an opportunity to reflect on the complexities of the HER and OER under mild pH conditions and the insights needed to build a strong conceptual framework to better understand them.

Methods

Materials

All chemicals used were commercially available and were used without further purification: potassium hydroxide (≥85%, Sigma-Aldrich), perchloric acid (70%, Sigma-Aldrich), potassium sulfate (99.8%, Sigma-Aldrich), sodium perchlorate (>98%, Sigma-Aldrich), sulfuric acid (98%, Sigma-Aldrich), acetic acid (99.7%, Sigma-Aldrich), potassium acetate (≥99.0%, Sigma-Aldrich), potassium phosphate dibasic (99.6%, Fischer Scientific), boric acid (≥99.5%, Sigma), nickel(II) nitrate hexahydrate (99%, Acros), potassium nitrate (99%, Alfa Aesar), ammonium sulfate (≥99.0%, Sigma-Aldrich), ruthenium(IV) oxide (99.9%, Sigma-Aldrich), super C65 carbon black (Timical) and Nafion solution (5 wt%, Sigma-Aldrich). Electrode polishing alumina suspension (0.05 µm, BASi). Deionized water (Barnstead E-pure water purification system; resistivity, >18 MΩ cm) was used to prepare all solutions.

Preparation of RuO_2 electrodes

First, 10 mg RuO_2 and 2 mg C65 carbon black were added to 1 ml deionized water containing 50 µl Nafion solution (5 wt%). The mixture was sonicated for 30 min to obtain a well-dispersed catalyst ink. Then, 10 µl catalyst ink was drop-cast onto a freshly polished gold RDE, and dried at 60 °C for 3 min to form a RuO_2 thin-film working electrode.

Deposition of $Ni(OH)_2$ electrocatalysts

The $Ni(OH)_2$ electrocatalysts used for ammonia oxidation were prepared through an established electrodeposition technique in which nitrate is reduced at the working electrode, leading to an increase in the local pH that causes Ni^{2+} to precipitate out as $Ni(OH)_2$[41]. This was done with a three-electrode set-up using a fluorine-doped tin oxide (FTO) working electrode, a Ag/AgCl reference electrode and a platinum counter-electrode, and was controlled using an SP-200 potentiostat/EIS (BioLogic Science Instruments). The FTO working electrode was prepared by attaching copper tape to the top of a 2.5 cm × 1 cm FTO plate to provide electrical contact, then masking the electrode with electroplating tape (3M Company) with a 0.5-cm^2 hole punched in it. The platinum electrode was prepared by sputter coating a cleaned glass slide with a 20-nm titanium adhesion layer followed by a 100-nm platinum layer. The electrodeposition was achieved by maintaining a -0.25 mA cm^{-2} current density for 45 s with a deposition solution consisting of 10 mM $Ni(NO_3)_2{\cdot}6H_2O$ and 30 mM KNO_3. The electrodeposited $Ni(OH)_2$ films were then rinsed with >18 MΩ cm water and dried with an air stream.

Solution preparation

Unbuffered solutions in the pH range from 0 to 4 were prepared by adding the appropriate volume of $HClO_4$ needed to produce the desired pH to a 1 M solution of $NaClO_4$. A pH probe (Fisher Scientific, accuTupH) was then used to confirm this resulted in the desired pH. For pHs 5–12, the solutions were prepared by starting with a 0.5 M K_2SO_4 solution and then adding H_2SO_4 or KOH as needed until the desired pH was reached as determined by a pH probe. For pH 13 and 14 an appropriate amount mass of KOH was added to a 0.2 M K_2SO_4 solution to produce the desired pH. These solutions were then immediately used to perform the electrochemical experiments.

For buffered solutions, different buffer systems were chosen based on the pH we wished to maintain. A 0.5 M K_2SO_4/K_2HSO_4 buffer was used for pH 0–3, a 0.5 M potassium acetate/acetic acid buffer was used for pH 4–5, a 0.5 M Na_2HPO_4/NaH_2PO_4 buffer was used for pH 6–8, a 0.5 M potassium borate/boric acid buffer was used for pH 9–10, and a 0.5 M Na_3PO_4/Na_2HPO_4 buffer was used for pH 11–13. The pH 14 solution was not buffered because the large OH^- concentration made doing so unnecessary. In addition to the buffer ion, 0.2 M K_2SO_4 was added to all the solutions (except for the 0.5 M sulfate ones) to ensure they had a high ionic conductivity and to make them more similar to the unbuffered solutions which used K_2SO_4 as the supporting ion (for pH 4 and above).

The ammonia solution was prepared by starting with 0.5 M K_2SO_4, and adding 0, 15, 20 and 30 mM ammonium sulfate followed by adding KOH until the desired pH was reached as determined by a pH probe. Borate buffer solution for comparison was prepared by using 0, 15, 20 and 30 mM boric acid instead of ammonium sulfate.

RDE experiments

RDE experiments were conducted with a BASi RDE-2 Cell Stand using a three-electrode set-up. An Ag/AgCl (4 M KCl) electrode was used as the reference electrode and a platinum wire electrode as the counter-electrode. The electrochemical experiments were controlled using a VSP multichannel potentiostat (BioLogic). For the HER, the working electrode was either platinum (BASi, 3.0 mm diameter) or gold (BASi, 3.0 mm diameter). Prior to being used for electrochemical experiments, the working electrodes were polished using figure-of-eight motions for approximately 2 min on a microcloth polishing pad onto which had been added a slurry of polishing alumina. For the OER, the working electrode was the RuO_2 thin-film electrode as described above.

When performing the HER, H_2 was bubbled into the solution, and while performing the OER, O_2 was bubbled into the solution. All LSVs in this study are presented without *iR* corrections because the ample supporting electrolyte contained in all solutions ensured sufficiently low and comparable solution resistances such that *iR* corrections do not affect the discussions in this study. For example, the uncompensated solution resistances (R_u) of the unbuffered pH 1, 2, 3, 7, 12 and 13 solutions were 15.4, 21.6, 21.8, 18.0, 17.8 and 25.6 Ω, respectively. Note that while all current is reported in current density (mA cm^{-2}) in this study, the actual experimental current obtained by the RDE electrode with an area of 0.07 cm^2 is 14 times lower. The R_u was measured by electrochemical impedance spectroscopy at 200 kHz–0.5 Hz with an a.c. voltage of 10 mV at open-circuit potential.

LSVs obtained with copper, silver and indium

The copper, silver and indium electrodes were prepared by cutting metal foils into 3 cm × 1.3 cm strips and masking the front and back side of the metal foil with Teflon tape to expose an area of 1 cm × 1 cm on the front side. Copper foil (99.9%, Nimrod Copper), indium foil (99.99%, Alfa Aesar) and silver foil (99.99%, Alfa Aesar) were used. Before LSV measurements, the surface oxide layers on the foil electrodes were removed by acid etching. The copper foil electrode was immersed in 10 wt% H_2SO_4 for 10 s; silver and indium foils were immersed in 37% HCl for 10 s. After acid etching, the electrodes were rinsed with deionized water and dried using a N_2 flow. LSVs were obtained in a three-electrode set-up using the copper, silver or indium electrode as the working electrode with a graphite counter-electrode and a Ag/AgCl (4 M KCl) reference electrode. The solution was saturated with H_2 prior to each LSV measurement for the HER. During the LSV measurement in an unstirred solution, H_2 was not purged in the solution so as not to add convective mass transport. Instead, H_2 was purged in the headspace of a semi-sealed cell, creating a H_2 blanket.

Ammonia oxidation

The ammonia oxidation experiments were achieved using the same three-electrode set-up used for the electrodeposition described above but with $Ni(OH)_2$ instead of bare FTO as the working electrode. The ammonia solution was contained in a glass single-cell compartment. LSVs were collected by sweeping from the open circuit in the positive direction. For experiments where stirring was needed, this was achieved by adding a magnetic stir bar to the ammonia solution and using a stir plate.

Data availability

The source data files for the plots contained in the current study are attached. Source data are provided with this paper.

References

1. Roger, I., Shipman, M. A. & Symes, M. D. Earth-abundant catalysts for electrochemical and photoelectrochemical water splitting. *Nat. Rev. Chem.* **1**, 0003 (2017).
2. Cook, T. R. et al. Solar energy supply and storage for the legacy and nonlegacy worlds. *Chem. Rev.* **110**, 6474–6502 (2010).
3. Li, X., Hao, X., Abudula, A. & Guan, G. Nanostructured catalysts for electrochemical water splitting: current state and prospects. *J. Mater. Chem. A* **4**, 11973–12000 (2016).
4. Xia, R., Overa, S. & Jiao, F. Emerging electrochemical processes to decarbonize the chemical industry. *JACS Au* **2**, 1054–1070 (2022).
5. Martín, A. J. & Pérez-Ramírez, J. Heading to distributed electrocatalytic conversion of small abundant molecules into fuels, chemicals, and fertilizers. *Joule* **3**, 2602–2621 (2019).
6. Bender, M. T., Yuan, X., Goetz, M. K. & Choi, K. S. Electrochemical hydrogenation, hydrogenolysis, and dehydrogenation for reductive and oxidative biomass upgrading using 5-hydroxymethylfurfural as a model system. *ACS Catal.* **12**, 12349–12368 (2022).
7. Nitopi, S. et al. Progress and perspectives of electrochemical CO_2 reduction on copper in aqueous electrolyte. *Chem. Rev.* **119**, 7610–7672 (2019).
8. Goetz, M. K., Bender, M. T. & Choi, K.-S. Predictive control of selective secondary alcohol oxidation of glycerol on NiOOH. *Nat. Commun.* **13**, 5848 (2022).
9. Varela, A. S. et al. pH effects on the selectivity of the electrocatalytic CO_2 reduction on graphene-embedded Fe–N–C motifs: bridging concepts between molecular homogeneous and solid-state heterogeneous catalysis. *ACS Energy Lett.* **3**, 812–817 (2018).
10. Yuan, X., Lee, K., Eisenberg, J. B., Schmidt, J. R. & Choi, K.-S. Selective deoxygenation of biomass-derived carbonyl compounds on Zn via electrochemical Clemmensen reduction. *Nat. Catal.* **7**, 43–54 (2024).
11. Wang, J. et al. Ambient ammonia synthesis via palladium-catalyzed electrohydrogenation of dinitrogen at low overpotential. *Nat. Commun.* **9**, 1795 (2018).
12. Subbaraman, R. et al. Trends in activity for the water electrolyser reactions on 3*d* M(Ni,Co,Fe,Mn) hydr(oxy)oxide catalysts. *Nat. Mater.* **11**, 550–557 (2012).
13. Strmcnik, D. et al. Improving the hydrogen oxidation reaction rate by promotion of hydroxyl adsorption. *Nat. Chem.* **5**, 300–306 (2013).
14. Durst, J. et al. New insights into the electrochemical hydrogen oxidation and evolution reaction mechanism. *Energy Environ. Sci.* **7**, 2255–2260 (2014).
15. Strmcnik, D., Lopes, P. P., Genorio, B., Stamenkovic, V. R. & Markovic, N. M. Design principles for hydrogen evolution reaction catalyst materials. *Nano Energy* **29**, 29–36 (2016).
16. Lamoureux, P. S., Singh, A. R. & Chan, K. pH effects on hydrogen evolution and oxidation over Pt(111): insights from first-principles. *ACS Catal.* **9**, 6194–6201 (2019).
17. Govindarajan, N., Xu, A. & Chan, K. How pH affects electrochemical processes. *Science* **375**, 379–380 (2022).
18. Jung, O., Jackson, M. N., Bisbey, R. P., Kogan, N. E. & Surendranath, Y. Innocent buffers reveal the intrinsic pH- and coverage-dependent kinetics of the hydrogen evolution reaction on noble metals. *Joule* **6**, 476–493 (2022).
19. McCrum, I. T. & Koper, M. T. M. The role of adsorbed hydroxide in hydrogen evolution reaction kinetics on modified platinum. *Nat. Energy* **5**, 891–899 (2020).
20. Zhou, Z. et al. Electrocatalytic hydrogen evolution under neutral pH conditions: current understandings, recent advances, and future prospects. *Energy Environ. Sci.* **13**, 3185–3206 (2020).
21. Liu, L., Liu, Y. & Liu, C. enhancing the understanding of hydrogen evolution and oxidation reactions on Pt(111) through ab initio simulation of electrode/electrolyte kinetics. *J. Am. Chem. Soc.* **142**, 4985–4989 (2020).
22. Auinger, M. et al. Near-surface ion distribution and buffer effects during electrochemical reactions. *Phys. Chem. Chem. Phys.* **13**, 16384–16394 (2011).
23. Grozovski, V., Vesztergom, S., Láng, G. G. & Broekmann, P. Electrochemical hydrogen evolution: H^+ or H_2O reduction? A rotating disk electrode study. *J. Electrochem. Soc.* **164**, E3171–E3178 (2017).
24. Su, L. et al. Electric-double-layer origin of the kinetic pH effect of hydrogen electrocatalysis revealed by a universal hydroxide adsorption-dependent inflection-point behavior. *J. Am. Chem. Soc.* **145**, 12051–12058 (2023).
25. Li, J., Stenlid, J. H., Ludwig, T., Lamoureux, P. S. & Abild-Pedersen, F. Modeling potential-dependent electrochemical activation barriers: revisiting the alkaline hydrogen evolution reaction. *J. Am. Chem. Soc.* **143**, 19341–19355 (2021).
26. Sheng, W., Gasteiger, H. A. & Shao-Horn, Y. Hydrogen oxidation and evolution reaction kinetics on platinum: acid vs alkaline electrolytes. *J. Electrochem. Soc.* **157**, B1529–B1536 (2010).

27. Sheng, W., Myint, M., Chen, J. G. & Yan, Y. Correlating the hydrogen evolution reaction activity in alkaline electrolytes with the hydrogen binding energy on monometallic surfaces. *Energy Environ. Sci.* **6**, 1509–1512 (2013).
28. Ma, W. et al. Electrocatalytic reduction of CO_2 and CO to multi-carbon compounds over Cu-based catalysts. *Chem. Soc. Rev.* **50**, 12897–12914 (2021).
29. Xiong, Y. et al. Electrochemical nitrate reduction: ammonia synthesis and the beyond. *Adv. Mater.* **36**, 2304021 (2024).
30. Sun, D., Xu, X., Qin, Y., Jiang, S. P. & Shao, Z. Rational design of Ag-based catalysts for the electrochemical CO_2 reduction to CO: a review. *ChemSusChem* **13**, 39–58 (2020).
31. Hoffman, Z. B., Gray, T. S., Moraveck, K. B., Gunnoe, T. B. & Zangari, G. Electrochemical reduction of carbon dioxide to syngas and formate at dendritic copper–indium electrocatalysts. *ACS Catal.* **7**, 5381–5390 (2017).
32. Jackson, M. N., Jung, O., Lamotte, H. C. & Surendranath, Y. Donor-dependent promotion of interfacial proton-coupled electron transfer in aqueous electrocatalysis. *ACS Catal.* **9**, 3737–3743 (2019).
33. Clary, K. E. et al. Increasing the rate of the hydrogen evolution reaction in neutral water with protic buffer electrolytes. *Proc. Natl Acad. Sci.* **117**, 32947–32953 (2020).
34. Ovalle, V. J. & Waegele, M. M. Influence of pH and proton donor/acceptor identity on electrocatalysis in aqueous media. *J. Phys. Chem. C.* **125**, 18567–18578 (2021).
35. Dionigi, F. & Strasser, P. NiFe-based (oxy)hydroxide catalysts for oxygen evolution reaction in non-acidic electrolytes. *Adv. Energy Mater.* **6**, 1600621 (2016).
36. Kapałka, A. et al. Electrochemical behavior of ammonia at Ni/$Ni(OH)_2$ electrode. *Electrochem. Commun.* **12**, 18–21 (2010).
37. Allagui, A., Sarfraz, S., Middleton, B., Almomani, F. & Baranova, E. A. Ammonia electrooxidation on NiPd nanoparticles in alkaline media: effect of pH and concentration. *ECS Trans.* **50**, 1897–1906 (2013).
38. Allagui, A., Sarfraz, S., Ntais, S. & Baranova, E. A. Electrochemical behavior of ammonia on $Ni_{98}Pd_2$ nano-structured catalyst. *Int. J. Hydrogen Energy* **39**, 41–48 (2014).
39. Shih, Y.-J., Huang, Y.-H. & Huang, C. P. Electrocatalytic ammonia oxidation over a nickel foam electrode: role of $Ni(OH)_2$(s)-NiOOH(s) nanocatalysts. *Electrochim. Acta* **263**, 261–271 (2018).
40. Adli, N. M., Zhang, H., Mukherjee, S. & Wu, G. Review—ammonia oxidation electrocatalysis for hydrogen generation and fuel cells. *J. Electrochem. Soc.* **165**, J3130–J3147 (2018).
41. Kang, D. et al. Electrochemical synthesis of photoelectrodes and catalysts for use in solar water splitting. *Chem. Rev.* **115**, 12839–12887 (2015).

Acknowledgements

This work was support by the Division of Chemical Sciences, Geosciences, and Biosciences, Office of Basic Energy Sciences of the US Department of Energy through grant DE-SC0024211.

Author contributions

K.-S.C. and M.T.B. conceived the project. Under the supervision of K.-S.C., X.Y. and M.T.B. performed all experiments with the contribution of M.K. for HER LSVs with various metals. All authors discussed the results and contributed to writing the manuscript.

Competing interests

The authors declare no competing interests.

Additional information

Supplementary information The online version contains supplementary material available at https://doi.org/10.1038/s41929-025-01339-0.

Correspondence and requests for materials should be addressed to Kyoung-Shin Choi.

Peer review information *Nature Catalysis* thanks the anonymous reviewer(s) for their contribution to the peer review of this work.